THE JOURNAL OF PHYSICAL CHEMISTRY C

Article

Cite This: J. Phys. Chem. C 2018, 122, 4125−4132

pubs.acs.org/JPCC

Inorganic Aromaticity of Mn_6-Ring Cluster in Layered $Li(Ni_{0.5}Mn_{0.5})O_2$

Zongxiang Hu,† Jiaxin Zheng,† Chao Xin,† Gaofeng Teng, Yunxing Zuo, and Feng Pan*

School of Advanced Materials, Peking University, Shenzhen Graduate School, Shenzhen 518055, People's Republic of China

Supporting Information

ABSTRACT: Using ab initio calculations, here, we identified inorganic aromaticity of Mn_6-ring cluster in layered $Li(Ni_{0.5}Mn_{0.5})O_2$ with Ni/Li mixing. The comparison between delocalized orbitals Mn-d_{z^2} in Mn_6-ring and benzene-p_z uncovers the fundamental similarity between a local cluster and benzene in electronic behavior. We also demonstrate that the delocalized interactions between transition metals (TMs) play a great role in the formation of inorganic aromaticity of Mn_6-ring in layered TM $Li(Ni_{0.5}Mn_{0.5})O_2$ (with Ni/Li mixing) via a two-level hierarchy: (i) the same TM ions (here manganese) can interact with each other directly through delocalized orbitals Mn-d in Mn_6-ring, and the local symmetry can impose restrictions on this delocalization. The direct exchange interactions play an important role at this level. (ii) The anions, here oxygen, can match with these delocalized orbitals of d-manifold via bridged bonds to share their electrons with TM ions to create the superexchange interactions, which enable the formation of solid local cluster Mn_6O_{24}. The present findings broaden our knowledge about the interactions between transition metals and provide important factors on governing the local ordering in TM compounds.

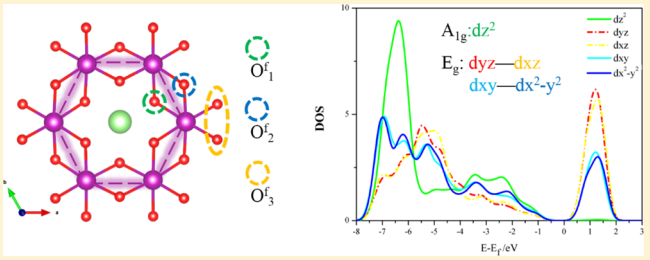

INTRODUCTION

Since the introduction of aromaticity on the structure of benzene by Kekulé's,[1] it has become one of the fascinating topics in chemistry, attracting continuous interests of both experimentalists and theoreticians over a century.[2−6] Although aromaticity is still a rather fuzzy concept, it is generally agreed that aromatic compounds are planar, cyclic, fully conjugated systems, which possess delocalized π-electrons. This cyclically delocalized and conjugate electronic structure confers special properties of aromatic compounds, including ring bond lengths, which are intermediate between normal single and double bonds, diamagnetic ring currents (diatropicity), and high thermodynamic stability.[2] Interestingly, besides benzene and its heterocyclic analogues (a CH group of benzene is formally replaced by an isoelectronic heteroatom, including pyridine, phosphabenzene, arsabenzene, pyrylium, thiabenzene, and even a transition metal (TM) and its associated ligands), aromatic metallic rings have also been observed in gas phases, such as $[M_2(GaH)_3]$ (M = Li, Na, K),[7] Al_4^-,[8] XAl_3^- (X = Si, Ge, Sn, Pb),[9] and Pn_5^- (Pn = P, As, Sb, Bi).[10] Furthermore, the first aromatic all-metal heterocycle, $[ZnBi_4]^{3-}$, was found in the metallic salt, K_6ZnBi_5, which has been synthesized and structurally characterized.[11]

Both previous experimental and theoretical investigations on the multiple-cation ordering/disordering in layered transition-metal (TM) oxides, which is a widely used cathode material for rechargeable lithium-ion batteries, demonstrated that the arrangement of cations does not employ a random configuration but an ordering pattern.[12−18] For examples, using high-resolution solid-state NMR, synchrotron X-ray diffraction, electron diffraction, and neutron diffraction studies, it is suggested that short-range in-plane ordering is almost universal in mixed transition-metal (NMC) layered oxides.[12,13,16] Combined with first-principles simulations, a well-characterized $2\sqrt{3}$-type structure model in $Li(Ni_{0.5}Mn_{0.5})O_2$ (without cobalt) with 8.7% Li/Ni exchange has been established: 6 manganese ions preferentially occupy a coordination ring (Mn_6) surrounding the central Li ion in the transition-metal layers, whereas 12 nickel ions tend to form the outer ring encircling the first ring.[13,14] This unique local coordination environment looks like a flower ordering with surprising 6-fold symmetry, and all of the local coordination environments could come into being an organized periodical structure. Subsequently, they found that the flowerlike structure transforms from the ground-state zigzag-ordered structure without Li/Ni disorder undergoing a phase transition over 550°.[19] Thus, concerns have been raised: does the Mn_6 ring in $Li(Ni_{0.5}Mn_{0.5})O_2$ show similar aromaticity to the C_6 ring in benzene both? If yes, then what is the origin to form the inorganic aromaticity for Mn_6 ring in layered $Li(Ni_{0.5}Mn_{0.5})O_2$?

Herein, using ab initio calculations, we investigate the electronic structure and the physicochemical origin of local Mn_6 ring in layered $Li(Ni_{0.5}Mn_{0.5})O_2$. By carefully surveying the symmetry and electronic structure of local units (Mn_6) in $Li(Ni_{0.5}Mn_{0.5})O_2$, it is found that such holistic d-electron behavior of Mn_6O_{24} cluster is indeed similar to the delocalized carbon-p_z (C-p_z) in benzene. Analogously, the delocalized interactions between metals contribute to local cation ordering

Received: November 6, 2017
Revised: January 30, 2018
Published: January 31, 2018

Downloaded via UNIV TOWN OF SHENZHEN on March 16, 2026 at 02:08:02 (UTC).
See https://pubs.acs.org/sharingguidelines for options on how to legitimately share published articles.

© 2018 American Chemical Society

DOI: 10.1021/acs.jpcc.7b10968
J. Phys. Chem. C 2018, 122, 4125−4132

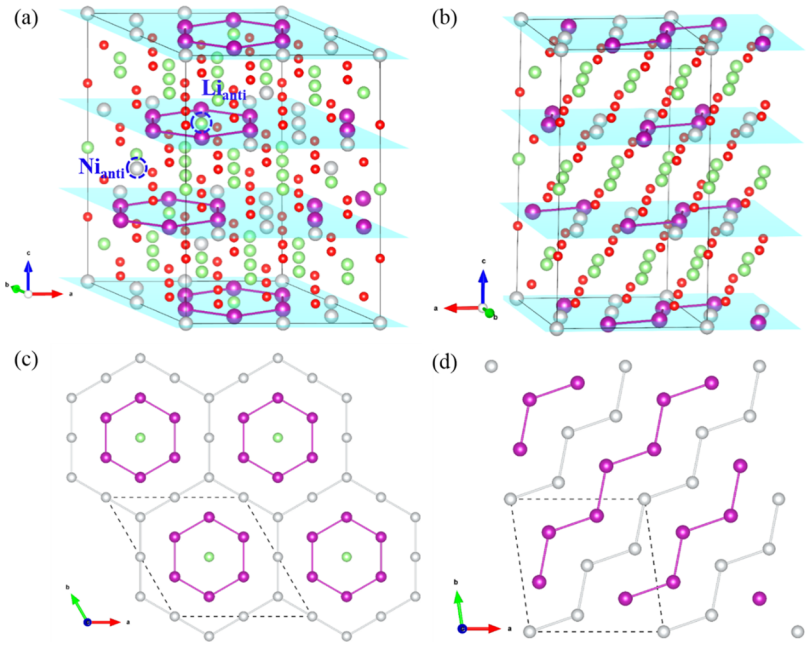

Figure 1. (a) Structure model of flowerlike configuration with anti-Ni (Ni_a); (b) structure model of zigzag configuration; (c) in-plane arrangement of TM in flowerlike configuration; and (d) in-plane arrangements of TM in zigzag configuration. The purple, silvery, green, and red spheres represent Mn, Ni, Li, and O elements, respectively.

and aromaticity of Mn_6-ring with 6-fold symmetry in $Li(Ni_{0.5}Mn_{0.5})O_2$. We also found that a delocalized mechanism can promote the formation of Mn_6 ring via a two-level hierarchy of interaction: (i) the same TM ions (here manganese) can interact with each other directly through delocalized orbitals Mn-d_{z^2} in Mn_6 ring, and the local symmetry can impose restrictions on this delocalization. The direct exchange interactions play an important role at this level. (ii) The anions, here oxygen, can match with these delocalized orbitals of d-manifold via bridged bonds to share their electrons with TM ions to create the superexchange interactions, which enable the formation of solid local cluster Mn_6O_{24}. It should also be noted that, if there is no Li/Ni exchange, then Ni centered in the clusters can weaken Mn−O bonding and jeopardize the existence of the clusters.

RESULTS AND DISCUSSION

Aromaticity in Structure Characteristic. According to previous studies, the most energetic favorable configurations, flowerlike and zigzag structures, are taken into account in $Li(Ni_{0.5}Mn_{0.5})O_2$.[13,20] All structures $Li(Ni_{0.5}Mn_{0.5})O_2$ built in this work are layered structures with space group $R\bar{3}m$, as the α-$NaFeO_2$ model. Figure 1 shows the supercells (Figure 1a,b) and the corresponding in-plane arrangements (Figure 1c,d). There are three layers of TM and three layers of Li-ions in each supercell. Stacking sequences of in-plane ordering perpendicular to the layers of these supercells adopt a stacking sequence of *abcabc*... along the c_{hex} axis. For flowerlike structure, the in-plane dimension with 8.7% Li/Ni exchange possesses a $2\sqrt{3}a_{hex} \times 2\sqrt{3}a_{hex}$ ordering. The supercells contain 24 and 36 formula units of $Li(Ni_{0.5}Mn_{0.5})O_2$ for zigzag and flowerlike ordering structures, respectively. All calculations were performed by GGA + *U* method, which integrates the generalized gradient approximation (GGA) with an on-site Coulomb potential for the d-electronics.[21] The values of the Hubbard-*U* parameters for Ni and Mn were determined from previous computational work.[15] We employed the reported effective *U* values 5.96 and 5.10 eV for Ni and Mn ions, respectively. For reasons that the values of *U* are system-dependent and can affect results of electronic structures, we also performed hybrid functional calculation to verify the reliability of electronic structure obtained by GGA + *U* calculations. The results obtained by HSE06 calculation are in accordance with our GGA + *U* results (for detailed discussion, see supplement of Computational Methods in Supporting Information). The calculated lattice parameters of these supercells with different magnetic configurations and the corresponding magnetic moments are consistent with previous calculations and close to experimental data (Table S1).[20] Figure S1 shows the magnetic configurations applied for calculation. The energies of zigzag, flowerlike structure with different magnetic configurations are shown in Table S2. It can be seen that for all atomic structures the ferrimagnetic configurations are energy-favorable. The absence of Jahn−Teller active Mn^{3+} and Ni^{3+} is in accordance with the calculated magnetic moments.[22] By comparing the energies of zigzag and flowerlike structures, we find that the energy of the zigzag structure is lower than that of the flowerlike structure, which is consistent with previous calculations.[13] The zigzag-like state with no Li/Ni exchange (−23.05951 eV/FU) is energy-favorable than the flowerlike state (−23.03169 eV/FU), indicating higher stability at low temperature. However, after taking 8.3% Li/Ni mixing into consideration, it is revealed that the energy of the zigzag structure with identical Li/Ni mixing is higher than that of the flowerlike structure. Thus, when Li/Ni exchange occurs, the flowerlike structure is more energy-favorable (12.8 meV/FU) than the zigzag structure, so the zigzag configuration would undergo phase transition and transform to the more stable flowerlike configuration with increasing temperature. The results are in accordance with previous theoretical works by DFT calculations and Monte Carlo (MC) simulations.[13,19]

DOI: 10.1021/acs.jpcc.7b10968
J. Phys. Chem. C 2018, 122, 4125−4132

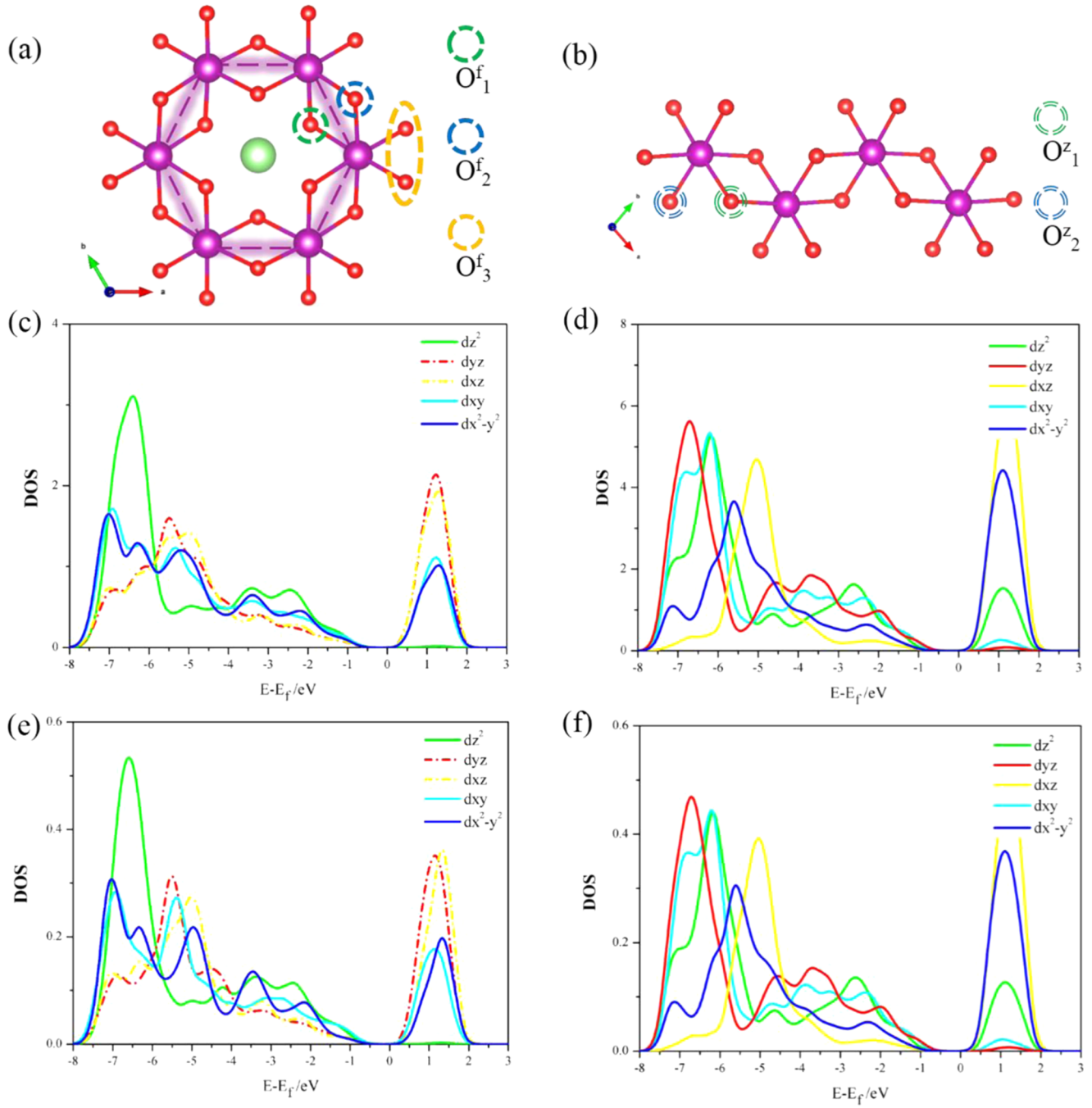

Figure 2. (a) Hypothetic Mn_6O_{24} cluster in flowerlike configuration. (b) Structure fragment of Mn zigzag chain. (c) Projected density of state (PDOS) of flowerlike configuration along the highest symmetry axis of the h-cluster. (d) PDOS of zigzag configuration along the highest symmetry axis of the MnO chain. (e) PDOS of individual Mn in Mn_6-ring. (f) The PDOS of individual Mn in MnO chain.

Figure 2a,b shows hypothetic clusters (h-cluster) extracted from flowerlike and zigzag structures, respectively. For the flowerlike configuration with Li/Ni mixing, there are six Mn (Mn_6) rings with one Li in the center in Mn_6O_{24} h-cluster coordinated by O groups, whereas there are Mn-chains in zigzag structures. According to O local environments (or lengths of Mn−O bonds), the O in Mn_6O_{24} h-cluster can be divided into three groups: O^f_1 (connected with two Mn and one Li), O^f_2 (connected with two Mn and one Ni), and O^f_3 (connected with one Mn and two Ni), as shown in Figures 2a and S2a. The lengths of Mn−O bonds are nearly identical in the same group but different in the three groups, with 1.980, 1.958, and 1.921 Å, respectively. The outmost O^f_3 ring of Mn_6O_{24} shows the shortest bonds, indicating that there is a real cluster shrinking as a whole to improve the stability. We then calculated the electron localization function (ELF) of the flowerlike configuration (Figure S3) and found that Mn_6O_{24} h-cluster can be viewed as six Mn coordinated by these three O groups. By contrast, there are only two environments for O in the zigzag structure (connected with two Mn and one or two Ni), as shown in Figures 2b and S2b. The O^z_2 linked to two Ni have shorter Mn−O bonds (1.925 Å), the same as O^f_3 in flowerlike structure. The Mn−O^z_1 bonding to two Mn have unequal lengths of bonds, with lengths of 1.953 and 1.987 Å,

DOI: 10.1021/acs.jpcc.7b10968
J. Phys. Chem. C 2018, 122, 4125−4132

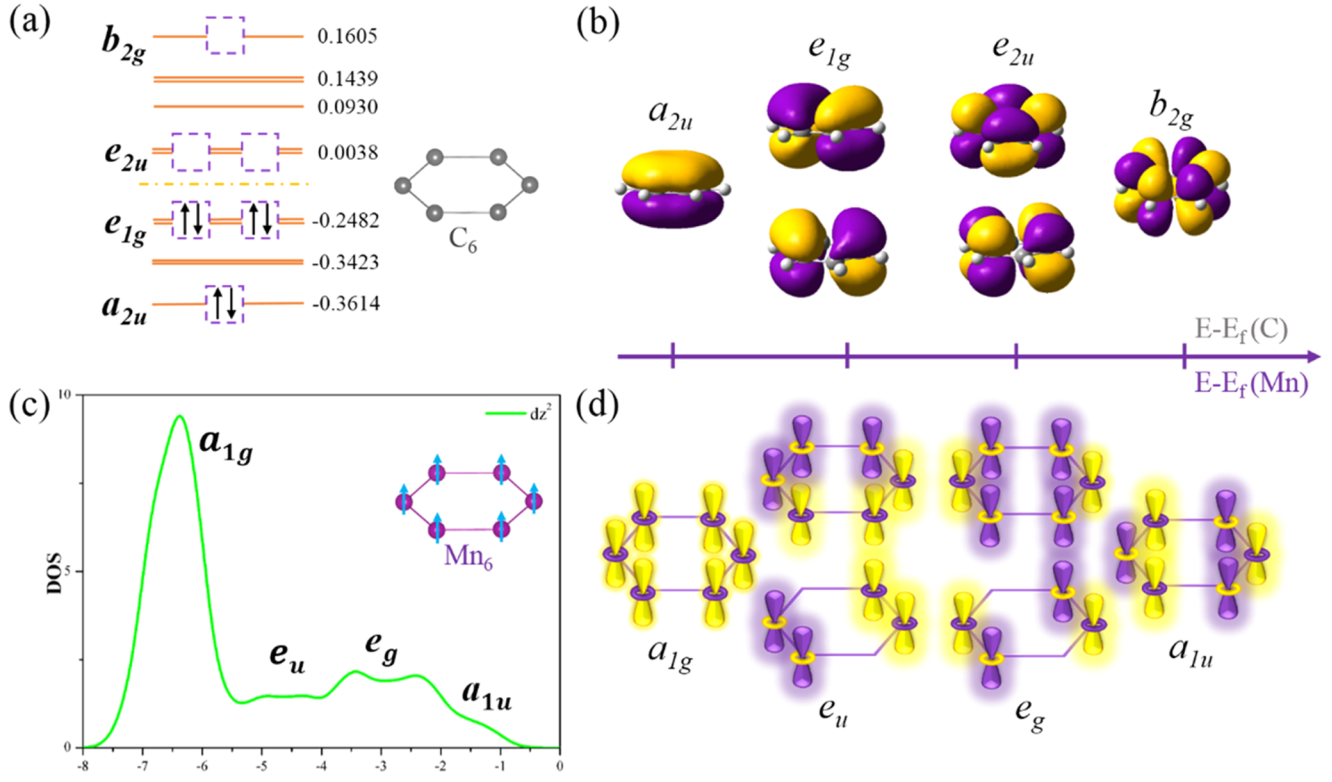

Figure 3. (a) Energy levels of C-p_z in benzene. (b) Delocalized orbitals of C-p_z, including two singlet states (a_{2g}, b_{2u}) and two doublet states (e_{1g}, e_{2u}). (c) PDOS (projected density of states) of Mn-d_{z^2} orbitals in flowerlike configuration. (d) Delocalized orbitals of Mn-d_{z^2} arranged in energy, including two singlet states (a_{1g}, a_{1u}) and two doublet states (e_u, e_g). The yellow parts of orbitals represent positive wavefunction, and the purple parts of orbitals represent negative wavefunction.

respectively, arranged alternately along the Mn−O zigzag chain. The distances of six Mn−Mn bonds in the Mn_6O_{24} cluster of the flowerlike structure are about 2.898 Å (which would be distorted 2.937 Å when it is near the upper and lower antisite-Ni; for detailed discussion, see Section S3 in Supporting Information), which are shorter than that in the zigzag structures (2.946 Å) to show a more compact tendency, which is analogous to six carbon−carbon (C−C) bonds in benzene with congruent length (1.40 Å) shorter than a single bond (1.47 Å) but greater than a double bond (1.35 Å). This intermediate bond length is consistent with electron delocalization: the electrons for C−C bonding are distributed equally between each of the six carbon atoms. Lengths of Mn−O in flowerlike structure are shorter than th in zigzag structure.Thus, form structure analogous, Mn_6-ring in flowerlike structure is similar to C_6-ring in benzene with aromaticity in structure characteristic, whereas Mn-chain in zigzag structure for is similar to C-chain of olefin and alkane in organic chemistry.

Aromaticity in Electronic Behavior. Electronic structures of Mn_6-ring of Mn_6O_{24} cluster in flower structure and Mn−Mn bonds in zigzag configuration are further analyzed. The projected density of states (PDOSs) of the Mn majority-spin d states of the two h-clusters is shown in Figure 2c,d. From the PDOS of Mn_6-ring, it can be seen that the d_{yz} states overlap with the d_{xz} states in the whole energy range, and meanwhile, the d_{xy} and $d_{x^2-y^2}$ states also superpose mutually through total energy interval, letting d_{z^2} states alone. The d states overlapping with each other are degenerate

$$\begin{cases} d_{z^2} \\ d_{xz},\ d_{yz} \\ d_{x^2-y^2},\ d_{xy} \end{cases}$$

We further checked the PDOS of individual Mn in Mn_6-ring (Figure 2e): the PDOS of individual Mn shows evident distinctions lacking degeneracies of d states that Mn_6-ring as a whole has. This suggests that the degeneracy is an inseparable nature of whole for Mn_6-ring due to entanglements between Mn cations. By contrast, from the PDOS of Mn-chain in zigzag structure (Figure 2d), it is found that its Mn-d states do not show high degeneracy compared to the flowerlike structure. In addition, the congruence between PDOS of individual Mn and all Mn of Mn-chain for the zigzag configuration further demonstrates that total behaviors of Mn cations of Mn-chain are merely linear additivity of individual Mn cation (Figure 2f), showing an obvious difference from the Mn_6-ring in flowerlike configuration. In other words, Mn cations of Mn-chain in the zigzag chain are comparatively isolated. A classical organic chemical picture of benzene and olefin might help us to understand the difference between Mn_6-ring and Mn-chain: the same surplus C-p_z electrons, but closed high-symmetry C_6 enables more effective C-p_z delocalization than open low-symmetry C-chain. Similarly to organic aromaticity, Mn_6-ring also shows more delocalized d states to create conjugate π-electrons than Mn-chain due to the closed and high-symmetry system.

Ordinarily, we next estimate the degeneracy of energy level of Mn_6-ring through the symmetry directly and strictly. The symmetry of Mn_6O_{24} h-cluster belongs to point group D_{3d}, and

DOI: 10.1021/acs.jpcc.7b10968
J. Phys. Chem. C 2018, 122, 4125−4132

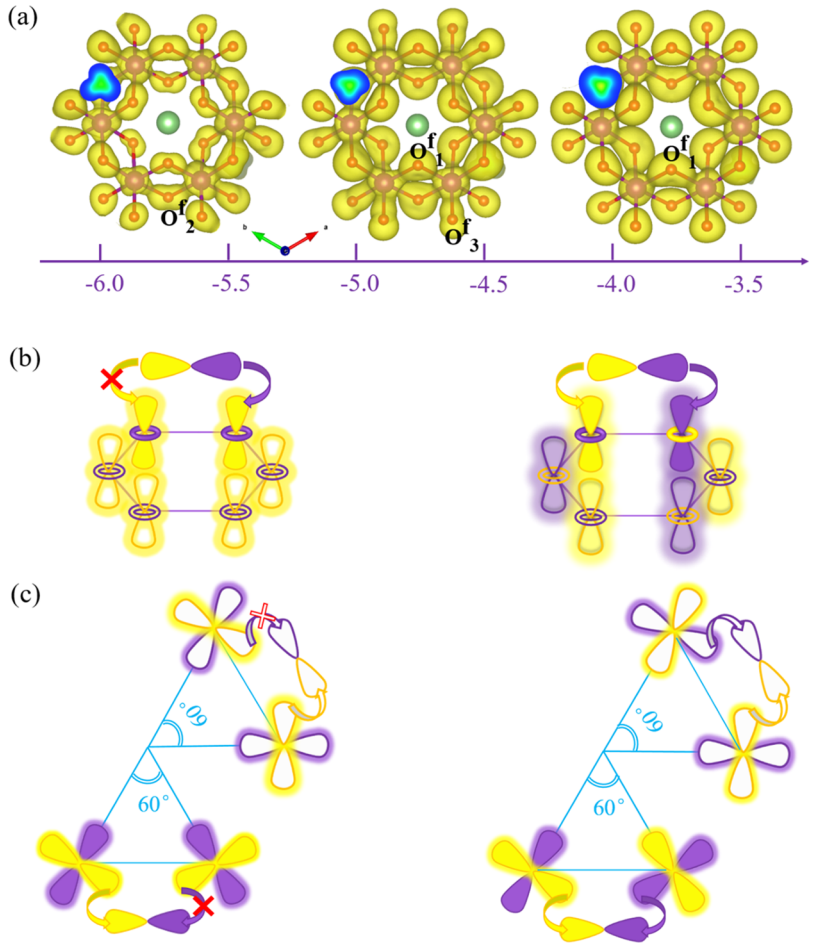

Figure 4. (a) Partial charge densities (PCD) arrange in energy from low to high. The varying patterns of PCD are restricted by O^f_1, O^f_2, O^f_3 groups. (b) Schematic diagram of interaction between delocalized d_{z^2} of Mn_6-ring and O groups. (c) Schematic diagram of interaction between delocalized $d_{x^2-y^2}$ of Mn_6-ring and O groups. The yellow parts of orbitals represent positive wavefunction, and the purple parts of orbitals represent negative wavefunction.

the schematic diagram of Mn_6O_{24} cluster is sketched with symmetry operations of point group D_{3d} explicitly (Figure S4). Decompositions of the d states according to group D_{3d} are shown in Table S3,[23] which can help us to directly estimate energy division of d states of a free atom interacted to electrostatic potential with D_{3d} symmetry. From the first column of Table S3, we can immediately get that orbitals d_{yz} and d_{xz} (also for d_{xy} and $d_{x^2-y^2}$) have the same energy distributions, labeled with 2-fold E_g representation, whereas d_{z^2} belongs to nondegenerate state labeled with A_{1g} representation. Interestingly, d states of Mn_6-ring also decompose to A_{1g} (d_{z^2}) and E_g (d_{yz}, d_{xz}; d_{xy}, $d_{x^2-y^2}$) groups just like one integral "atom". Obviously, the behaviors of d states originating from Mn_6-ring serve as a whole, where six Mn entangle with each other.

The degeneracy of d states of Mn_6-ring demonstrates the existence of a direct interaction between six Mn. Benzene is the typical representative of direct delocalized interaction. The six C-p_z orbitals in C_6 can interact with each other and produce new orbital assignments restricted by the D_{6h} symmetry of the C_6H_6 molecule. The energy levels and wavefunctions of delocalized C-p_z in benzene are shown in Figure 3a,b. The reassigned six orbitals are two nondegenerate states, a_{2u} and b_{2g}, and two doublet states, e_{1g} and e_{2u}. Each of these reassigned orbitals is contributed by part of original six C-p_z orbitals actually. In parallel, the hybridization between Mn d orbitals also changes energies of original d orbitals and generates new delocalized orbitals. We take A_{1g} (d_{z^2}) as an example to visualize specific forms of these delocalized orbitals. Figure 3c shows the PDOS of d_{z^2} states of Mn_6-ring. It can be seen that the hybridization of six d_{z^2} orbitals of Mn_6-ring can produce a_{1g}, e_u, e_g, and a_{1u} delocalized orbitals from left to right in energy. So, one-to-one corresponding relations between Mn-d_{z^2} and C-p_z can be built (Figure 3b,d). In energy intervals −5.5 to −4.0 eV and −3.5 to −2.0 eV, the doublet states e_u and e_g are split (Figure 3c) because of the distortion of Mn_6O_{24} cluster with the influence of antisite-Ni (for detailed discussion, see Section S3 in Supporting Information). The direct hybridization of E_g group, (d_{yz}, d_{xz}) and (d_{xy}, $d_{x^2-y^2}$), is examined furthermore (Figure S5), in which doublet states e_u and e_g are also split. It should be noted that the energy levels are broadened by crystal periodic potential and that different energy levels are not equally distributed. Although delocalization in Mn_6-ring is not exactly the same as in organic chemistry, aromaticities with conjugate π-electron delocalization based on the direct interaction in Mn_6-ring in Mn_6O_{24} and C_6-ring of benzene are similar.

Formation of d−pπ Bonding Enabling Aromaticity of Mn_6-Ring. Noticing the stronger overlapping between delocalized Mn_6-ring and O-p orbitals in Mn_6O_{24} cluster (Figure S3), to detail the interaction between d orbitals of Mn_6-

DOI: 10.1021/acs.jpcc.7b10968
J. Phys. Chem. C 2018, 122, 4125−4132

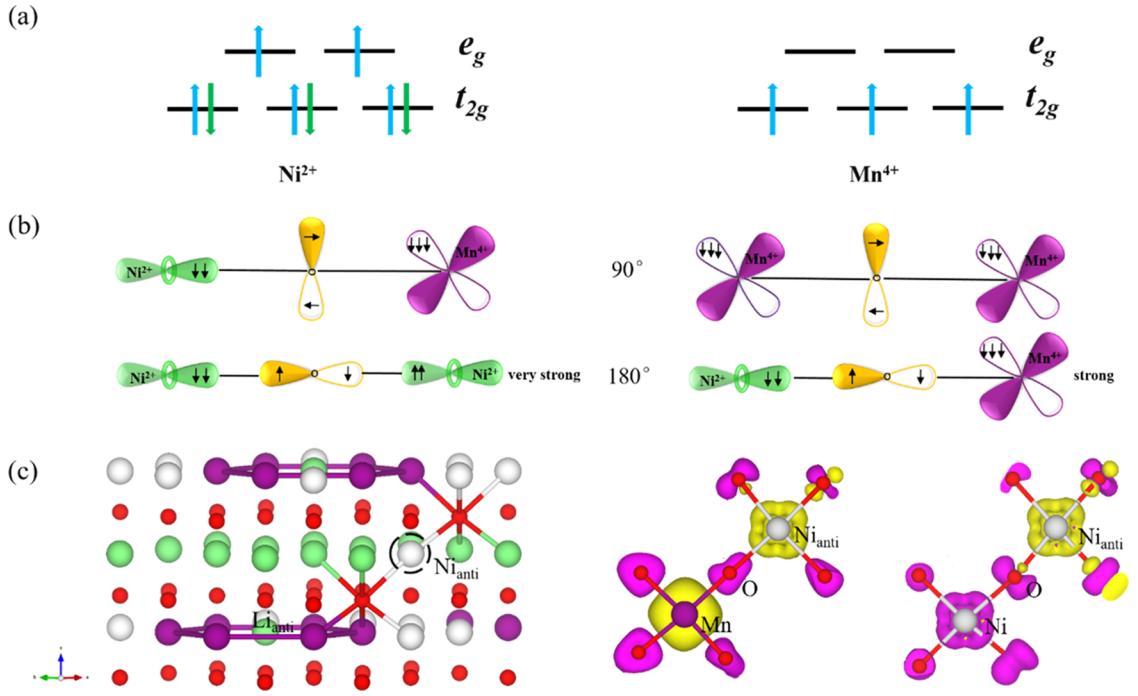

Figure 5. (a) Electronic configurations for TM ion in $Li(Ni_{1/2}Mn_{1/2})O_2$. (b) Schematic for 90 and 180° superexchanges. (c) Interlayered 180° superexchange interactions.

ring and O-p orbitals, we calculate the partial charge density (PCD) ranged in different energy intervals (Figure 4a). Interestingly, a particular bonding form can be seen in the PCD pictures for $Mn-O^f_1$ and $Mn-O^f_2$ bonds. The shape is similar to a bridge linking two adjacent Mn equally, which forms an effective $(d-p-d)\pi$ bonding. The distribution of this bonding is quite broad in energy. Figure 4b,c shows the schematic diagram of $(d-p-d)\pi$ bonding between delocalized Mn_6-ring and O groups. First, we take d_{z^2} orbitals to exemplify the bonding process (Figure 4b). Obviously, to form this bonding, dumbbell-shaped p orbitals of O^f_1 and O^f_2 should parallel two adjacent Mn. However, the two terminals of dumbbell are one positive and one negative, and the localized d_{z^2} orbitals cannot form this $(d-p-d)\pi$ bonding because negative terminal of p orbital always counteracts with positive d states (left part in Figure 4b). However, for reassigned orbitals of Mn in Mn_6-ring like a_{1u} (right part in Figure 4b), wavefunctions of adjacent Mn d_{z^2} states have opposite sign and exactly match to two terminals of p orbital bonding to two Mn equally. Figure 4c shows $d_{x^2-y^2}$ orbitals from this $(d-p-d)\pi$ bonding. The existence of $(d-p-d)\pi$ bonding in broad energy range is also due to the delocalized d states in broad energy range. At the position of peaks a_{1g} (below energy −7.0 eV), we cannot find $(d-p-d)\pi$ bonding because localized d states have a_{1g} symmetry. When we look into $Mn-O^f_3$ bonds, familiar images come to our minds, that is, the shape of σ bond ordinarily symmetrized with respect to rotation about the bond axis. As we know, the σ bond is the strongest bond, which explains why the outmost $Mn-O^f_3$ bonds are the shortest. So, Mn_6-ring can bond to O tightly through delocalized d states to generate "big conjugate $(d-p-d)\pi$-electron delocalization". We call this property of consolidating stability "aromaticity" to some extent.

Origin of Aromaticity of Mn_6-Ring. Electron spin coupling has been raised to describe an aromatic characteristic of benzene: the p_z in benzene are certainly localized, but aromaticity of this system arises from the symmetry coupling of electron spins around the carbon framework.[24] The reason why Mn-d states can delocalize with each other can be understood from the magnetic direct interaction between magnetic shells with electron spin coupling.[25] The d electrons can usually be delocalized in metals but localized in metallic oxides. Figure S6 shows the form of d-orbital division and electronic configuration of individual Mn^{4+} and Ni^{2+} octahedrally coordinated by six O. It can be seen that the e'_g orbitals spread toward ligand directly from the plots of e'_g orbitals, so their delocalizability usually have been isolated by O. In TM layers, the MO_6 (M = Mn or Ni) octahedra share edges, and itinerant electrons in the t'_{2g} orbitals directly spread to each other, making direct electronic exchange possible.[25] Thus, the delocalization is strengthened through magnetic exchange between half-filling t'_{2g} orbitals of Mn^{4+}, rather than Ni^{2+}. One would ask that, as the distance of Mn−Mn is almost twice as much as C−C length, what is the key factor to lead to the delocalization of Mn_6-ring to generate direct electronic exchange. Through electronic radial distribution for hydrogen-like atom, we note that the rate of decay of 3d electron is much lower than that of 2p electron (Figure S7) to lead to more broad delocalization. The bond lengths of some good conductors, such as Cu and Au, are usually 2.56−2.95 Å, much larger than C−C length about 1.4 Å. So, Mn−Mn length about 2.9 Å can be fitted to create direct electronic delocalization interactions.

Magnetic coupling based on spin electrons not only benefits direct interactions between Mn in Mn_6-ring, but also facilitates interactions between TM and O elements. The superexchange interaction is a strong ferromagnetic (FM)/antiferromagnetic (AF) coupling between two next-to-nearest neighbor transition metals through a nonmagnetic anion (Figure 5a,b).[26] The local Mn_6O_{24} clusters are connected by Ni through O. The superexchange interaction can lower the energy and consolidate the stability through ferrimagnetic configuration. The ELF plots

DOI: 10.1021/acs.jpcc.7b10968
J. Phys. Chem. C 2018, 122, 4125−4132

of FM and AF configurations also show that AF configuration can further motivate the activation of O (Figure S8). Combined with previous reports,[27,28] compared to Mn^{4+}, the d band moves down in energy for Ni^{2+}. The filling of e'_g band increases, and the antibonding oxygen-metal d states become more populated and weaker. So, Ni ions in the TM layer served as a median between Mn_6O_{24} clusters and do not need to bond so strongly as Mn-bonding in the cluster. However, a stronger interaction is the interlayered 180° superexchange interaction that can strengthen the structure, as shown in Figure 5c. As mentioned earlier, symmetry breaking of the Mn_6O_{24} cluster resulted by antisite-Ni (Ni_{anti}) are energetically favorable, in which the Ni_{anti} can interact with Mn_6-ring to be similar to the ferrocene (Fe sandwiched between two aromatic rings). Our calculation shows that antiparallel spins of 180° Ni_{anti}^{2+}−O−Ni^{2+} (parallel spins of 180° Ni_{anti}^{2+}−O−Mn^{4+}) can lower the energy by about 0.36 eV via comparing with parallel spins (antiparallel spins), which enhances the correlation between Mn_6O_{24} cluster with the entire structure. Thus, the origins of aromaticity of Mn_6-ring are direct interactions between Mn with the magnetic coupling of spin electrons and superexchange interaction of Mn−O−Mn with (d−p−d)π-electron delocalization in the Mn_6O_{24} cluster of flower structure.

Experimental Characterization on the Existence of Mn_6-Ring. Yoon et al. studied ordering in Li-$[Ni_xMn_{(2-x)/3}Li_{(1-2x)/3}]O_2$ (x = 1/10, 1/3, 1/2) by carefully analyzing the concentrations of different Li environments in the transition-metal layers obtained from NMR experiments and predicted from three different models for Li/Mn/Ni ordering.[13] They found that a random model cannot explain the experimental concentration of Li environments (e.g., Li-$(OMn)_6$, $Li(OMn)_5(ONi)$) from all samples and that the agreement of honeycomb model is good for the sample with lower Ni content. At high Ni content, Mn ions preferentially occupy sites surrounding Li and most is $Li(OMn)_6$ contain no Ni, indicating the tendency for Ni and Li avoidance. Combined with first-principles simulations, a long-range $2\sqrt{3}$-type structure model (flowerlike structure) in $Li(Ni_{0.5}Mn_{0.5})O_2$ with 8.7% Li/Ni exchange has been established: 6 manganese ions preferentially occupy coordination first ring surrounding the central Li ion in the transition-metal layers, whereas 12 nickel ions tend to form the second ring encircling the first ring.[13,14] Sophisticated neutron diffraction experiments provide further evidence for this flowerlike structure, although it is far from perfect.[29] However, characterizing detailed cation ordering is not easy in experiments. For most experiments, only average cation positions from an O_3 type of layered $LiCoO_2$ can be given for $Li(Ni_{0.5}Mn_{0.5})O_2$. Subsequently, using a joint cluster expansion and Monte Carlo (MC) simulation, Hinuma et al. found that the flowerlike structure transforms from ground-state zigzag-ordered structure without Li/Ni disorder undergoing an irreversible phase transition over 550°.[19] When over 620°, the flowerlike structure undergoes a reversible phase transition and changes to more disordered honeycomb structure, indicating that flowerlike structure is a low-energy stable phase. Chernova et al. also studied the magnetic properties of $Li(Ni_{0.5}Mn_{0.5})O_2$ and gave a good explanation for experimental data by assuming an imperfect flowerlike ordering.[25] Thus, experimental characterization of layered $Li(Ni_{0.5}Mn_{0.5})O_2$ supported the existence of Mn_6-ring.

CONCLUSIONS

In summary, using ab initio calculations, we identified an inorganic aromaticity of Mn_6-ring in layered $Li(Ni_{0.5}Mn_{0.5})O_2$ with Ni/Li mixing. The delocalized orbitals Mn-d_{z^2} in Mn_6-ring show similar electronic behavior to benzene-p_z. It is also found that the direct delocalized interactions combined with the superexchange interactions between TMs play a great role in forming the local Mn_6-ring in layered TM compounds. The delocalized interactions may exist in other transition-metal ring systems, and the new insight provides important factors on governing the local ordering with an inorganic aromaticity in TM compounds.

ASSOCIATED CONTENT

Supporting Information

The Supporting Information is available free of charge on the ACS Publications website at DOI: 10.1021/acs.jpcc.7b10968.

More details on first-principle calculations (PDF)

AUTHOR INFORMATION

Corresponding Author

*E-mail: panfeng@pkusz.edu.cn.

ORCID

Feng Pan: 0000-0002-8216-1339

Author Contributions

†Z.H. and J.Z., and C.X. contributed equally to this work.

Notes

The authors declare no competing financial interest.

ACKNOWLEDGMENTS

This work was financially supported by National Materials Genome Project (2016YFB0700600), the National Natural Science Foundation of China (No. 21603007 and 51672012), and Shenzhen Science and Technology Research Grant (No. JCYJ20150729111733470 and JCYJ20151015162256516).

REFERENCES

(1) Kekulé, A. Sur la constitution des substances aromatiques. *Bulletin mensuel de la Société Chimique de Paris* **1865**, *3*, 98.

(2) Bleeke, J. R. Metallabenzenes. *Chem. Rev.* **2001**, *101*, 1205−1228.

(3) Nyulászi, L. Aromaticity of phosphorus heterocycles. *Chem. Rev.* **2001**, *101*, 1229−1246.

(4) Minkin, V. I.; Minyaev, R. M. Cyclic aromatic systems with hypervalent centers. *Chem. Rev.* **2001**, *101*, 1247−1265.

(5) Katritzky, A. R.; Jug, K.; Oniciu, D. C. Quantitative measures of aromaticity for Mono-, Bi-, and tricyclic penta- and hexaatomic heteroaromatic ring systems and their interrelationships. *Chem. Rev.* **2001**, *101*, 1421−1449.

(6) Boldyrev, A. I.; Wang, L. S. All-metal aromaticity and antiaromaticity. *Chem. Rev.* **2005**, *105*, 3716−3757.

(7) Xie, Y.; Schreiner, P. R.; Schaefer, H. F.; Li, X. W.; Robinson, G. H. Are cyclogallenes $[M_2(GaH)_3]$ (M = Li, N, K) aromatic? *J. Am. Chem. Soc.* **1996**, *118*, 10635−10639.

(8) Li, X.; et al. Observation of All-Metal Aromatic Molecules. *Science* **2001**, *291*, 859−861.

(9) Li, X.; Zhang, H. F.; Wang, L. S.; Kuznetsov, A. E.; Cannon, N. A.; Boldyrev, A. I. Experimental and theoretical observations of aromaticity in heterocyclic XAl^{3-} (X = Si, Ge, Sn, Pb) systems. *Angew. Chem., Int. Ed.* **2001**, *40*, 1867−1870.

(10) Zhai, H. J.; Wang, L. S.; Kuznetsov, A. E.; Boldyrev, A. I. Probing the electronic structure and aromaticity of pentapnictogen cluster anions Pn_5^- (Pn = P, As, Sb, and Bi) using photoelectron

DOI: 10.1021/acs.jpcc.7b10968
J. Phys. Chem. C 2018, 122, 4125−4132

spectroscopy and ab initio calculations. *J. Phys. Chem. A* **2002**, *106*, 5600−5606.
(11) Qin, Q.; Zhou, L.; Wang, Y.; Sang, R.; Xu, L. $[ZnBi_4]^{3-}$ pentagon in K_6ZnBi_5: Aromatic all-metal heterocycle. *Inorg. Chem.* **2014**, *53*, 1266−1268.
(12) Meng, Y. S.; Ceder, G.; Grey, C. P.; Yoon, W. S.; Jiang, M.; Breger, J.; Shao-Horn, Y. Cation ordering in layered O3 Li-$[Ni_xLi_{1/3-2x/3}]Mn_{2/3-x/3}]O_2$ ($0 \leq x \leq 1/2$) compounds. *Chem. Mater.* **2005**, *17*, 2386−2394.
(13) Yoon, W.-S.; Iannopollo, S.; Grey, C. P.; Carlier, D.; Gorman, J.; Reed, J.; Ceder, G. Local Structure and Cation Ordering in O3 Lithium Nickel Manganese Oxides with Stoichiometry Li-$[Ni_xMn_{(2-x)/3}Li_{(1-2x)/3}]O_2$. *Electrochem. Solid-State Lett.* **2004**, *7*, A167.
(14) Van der Ven, A.; Ceder, G. Ordering in Lix$(Ni_{0.5}Mn_{0.5})O_2$ and its relation to charge capacity and electrochemical behavior in rechargeable lithium batteries. *Electrochem. Commun.* **2004**, *6*, 1045−1050.
(15) Dixit, M.; Kosa, M.; Lavi, O. S.; Markovsky, B.; Aurbach, D.; Major, D. T. Thermodynamic and kinetic studies of Li-$Ni_{0.5}Co_{0.2}Mn_{0.3}O_2$ as a positive electrode material for Li-ion batteries using first principles. *Phys. Chem. Chem. Phys.* **2016**, *18*, 6799−6812.
(16) Cahill, L. S.; Yin, S. C.; Samoson, A.; Heinmaa, I.; Nazar, L. F.; Goward, G. R. ^{6}Li NMR studies of cation disorder and transition metal ordering in $Li[Ni_{1/3}Mn_{1/3}Co_{1/3}]O_2$ using ultrafast magic angle spinning. *Chem. Mater.* **2005**, *17*, 6560−6566.
(17) Wei, Y.; Zheng, J.; Cui, S.; Song, X.; Su, Y.; Deng, W.; Wu, Z.; Wang, X.; Wang, W.; Rao, M.; et al. Kinetics Tuning of Li-Ion Diffusion in Layered $Li(Ni_xMn_yCo_z)O_2$. *J. Am. Chem. Soc.* **2015**, *137*, 8364−8367.
(18) Zheng, J.; Liu, T.; Hu, Z.; Wei, Y.; Song, X.; Ren, Y.; Wang, W.; Rao, M.; Lin, Y.; Chen, Z.; et al. Tuning of Thermal Stability in Layered $Li(Ni_xMn_yCo_z)O_2$. *J. Am. Chem. Soc.* **2016**, *138*, 13326−13334.
(19) Hinuma, Y.; Meng, Y. S.; Kang, K. S.; Ceder, G. Phase transitions in the $LiNi_{0.5}Mn_{0.5}O_2$ system with temperature. *Chem. Mater.* **2007**, *19*, 1790−1800.
(20) Dianat, A.; Seriani, N.; Bobeth, M.; Cuniberti, G. Effects of Al-doping on the properties of Li-Mn-Ni-O cathode materials for Li-ion batteries: an ab initio study. *J. Mater. Chem. A* **2013**, *1*, 9273−9280.
(21) Dudarev, S. L.; Botton, G. A.; Savrasov, S. Y.; Humphreys, C. J.; Sutton, A. P. Electron-energy-loss spectra and the structural stability of nickel oxide: An LSDA+U study. *Phys. Rev. B* **1998**, *57*, 1505−1509.
(22) Hwang, B. J.; Tsai, Y. W.; Carlier, D.; Ceder, G. A combined computational/experimental study on $LiNi_{1/3}Co_{1/3}Mn_{1/3}O_2$. *Chem. Mater.* **2003**, *15*, 3676−3682.
(23) Dresselhaus, M. S.; Dresselhaus, G.; Jorio, A. *Group Theory: Application to the Physics of Condensed Matter*; Springer: Berlin Heidelberg, 2007.
(24) Cooper, D. L.; Gerratt, J.; Raimondi, M. The Electronic-Structure Of the Benzene Molecule. *Nature* **1986**, *323*, 699−701.
(25) Chernova, N. A.; Ma, M.; Xiao, J.; Whittingham, M. S.; Breger, J.; Grey, C. P. Layered $Li_xNi_yMn_yCo_{1-2y}O_2$ cathodes for lithium ion batteries: Understanding local structure via magnetic properties. *Chem. Mater.* **2007**, *19*, 4682−4693.
(26) Kramers, H. A. The interaction between the magnetogenic atoms in a paramagnetic crystal. *Physica* **1934**, *1*, 182−192.
(27) Sun, H.; Zhao, K. J. Electronic Structure and Comparative Properties of $LiNi_xMn_yCo_zO_2$ Cathode Materials. *J. Phys. Chem. C* **2017**, *121*, 6002−6010.
(28) Xie, Y.; Saubanere, M.; Doublet, M. L. Requirements for reversible extra-capacity in Li-rich layered oxides for Li-ion batteries. *Energy Environ. Sci.* **2017**, *10*, 266−274.
(29) Bréger, J.; Dupré, N.; Chupas, P. J.; Lee, P. L.; Proffen, T.; Parise, J. B.; Grey, C. P. Short- and long-range order in the positive electrode material, $Li(NiMn)_{0.5}O_2$: A joint X-ray and neutron diffraction, pair distribution function analysis and NMR study. *J. Am. Chem. Soc.* **2005**, *127*, 7529−7537.

DOI: 10.1021/acs.jpcc.7b10968
J. Phys. Chem. C 2018, 122, 4125−4132